DANMARKS OG GRØNLANDS GEOLOGISKE UNDERSØGELSE RAPPORT 1997/35

# Quantitative NMR Measurements on Core Samples

## Tecnical Report for the EFP-95 Project: "Core Investigations by use of Different Physical Measurements" ENS Journal no. 1313/95-0007

Dan Olsen

GEOLOGICAL SURVEY OF DENMARK AND GREENLAND
MINISTRY OF ENVIRONMENT AND ENERGY

GEUS

DANMARKS OG GRØNLANDS GEOLOGISKE UNDERSØGELSE RAPPORT 1997/35

# Quantitative NMR Measurements on Core Samples

## Tecnical Report for the EFP-95 Project: "Core Investigations by use of Different Physical Measurements" ENS Journal no. 1313/95-0007

Dan Olsen

GEOLOGICAL SURVEY OF DENMARK AND GREENLAND
MINISTRY OF ENVIRONMENT AND ENERGY

GEUS

# Contents

# I. Summary

Within the frame of an EFP-95 project NMR methods for porosity determination in 2D, and for fluid saturation determination in 1D and 2D have been developed. The three methods have been developed and tested on cleaned core samples of chalk from the Danish North Sea.

The main restriction for the use of the methods is the inherently short T2 relaxation constants of rock samples. Referring to measurements conducted at 200 MHz, the 2D porosity determination method is applicable to sample material with T2 relaxation constants down to 5 ms. The 1D fluid saturation determination method is applicable to sample material with T2 relaxation constants down to 3 ms, while the 2D fluid saturation determination method is applicable to material with T2 relaxation constants down to 8 ms. In the case of the 2D methods these constraints as a minimum enables work on the majority of chalk samples of Maastrichtian age. The 1D fluid saturation determination method in addition is applicable to at least some chalk samples of Danian and pre-Maastrichtian age.

The spatial resolution of the 2D porosity determination method, the 1D fluid saturation methods, and the 2D fluid saturation method is respectively 0.8 mm, 0.8 mm and 2 mm. Reproducibility of pixel values is for all three methods 2 %-points.

# II. Introduction

**Project organization**

The project "Core Investigations by use of Different Physical Measurements" was initiated on March 1st, 1995 as a research project sponsored by the Ministry of Environment and Energy under the EFP-95 programme (J.no. 1313/95-0007). The project is a cooperation between Physics Department (Technical University of Denmark), Department of Automation (Technical University of Denmark), Department of Chemistry (Technical University of Denmark), Department of Chemical Engineering (Technical University of Denmark), and Danmarks og Grønlands Geologiske Undersøgelse (GEUS). Professor P. Ølgaard at Physics Department is project coordinator. The aim of the project is to develop and evaluate methods for determination of fluid saturation distributions and porosity distributions in rock samples from the hydrocarbon producing chalk formations of the Danish North Sea. Several physical methods are addressed in the project: A $\gamma$-transmission method is investigated at Physics Department and Department of Automation, an electrical impedance method is investigated at Department of Chemistry, an X-ray CT method is investigated at Department of Chemical Engineering, and an Nuclear Magnetic Resonance (NMR) method is investigated at GEUS. The present report is the final technical report for the latter subproject. A comparison of the methods will be presented in the final report of the project.

**Project rationale**

NMR is in common use for qualitative 2D visualization in biological systems. Biological tissue in general is well suited for NMR investigation because of high concentrations of protons combined with moderately high spin-spin relaxation constants (T2 constants). By contrast rock samples in general are much less suited, primarily because of low T2 constants. In the EU JOULE project JOUF-0019 GEUS developed methods for qualitative 2D visualizations of fluid saturation and porosity in suitable rock samples, and in the EFP-93 project J.no. 1313/93-0014 a quantitative method for obtaining 1D saturation profiles on rock samples was developed (Olsen et al., 1996). The present subproject has used the findings of these two projects to perform the following tasks:

1. A method for quantitative 2D mapping of porosity has been developed.
2. The EFP-93 method for quantitative 1D saturation profile determination has been considerably improved.
3. A method for quantitative 2D mapping of fluid saturation has been developed.

The methods are not applicable to all rock samples. They require that the samples have T2 relaxation constants above certain thresholds. They also require that the samples are saturated with a mixture of brine and oil, and do not contain a free gas phase. In the case of porosity mapping the sample must be fully saturated with

either brine or oil. In spite of the limitations it is expected that the methods will prove valuable within the field of core analysis. The 1D saturation profile method is at the time of writing successfully used by a research project under the EFP-96 programme.

An NMR scanner at the Danish Research Centre for Magnetic Resonance (DVMR) at Hvidovre Hospital in Copenhagen was used for the NMR work. DVMR is gratefully acknowledged for providing access to the scanner, and for invaluable discussions.

# III. Hardware and sample material

**Hardware**
A 4.7 T (200 MHz) SISCO experimental NMR scanner with a horizontal bore has been used in the project. The scanner is equipped with a 13 cm diameter insert gradient set, capable of producing magnetic gradient up to 100 mT/m individually along the directions X, Y and Z. Gradient riserate is $2*10^5$ mT/m*s.

Two RF (Radio Frequency) coils have been used, both of a slotted tube resonator design, and optimized for B1 homogeneity in the Z direction. One coil, Coil E, has good performance along a maximum length of approximately 90 mm, while the other coil, Coil F, has slightly inferior performance along a maximum length of approximately 110 mm. Coil F was specifically designed for use in the project, and a device for precise positioning of samples is mounted on the coil. The device allows movement of the sample in two orthogonal directions during NMR measurement. Both coils have physical inner diameters of 85 mm and maximum imageable diameters of approximately 60 mm.

**Sample material**
Sample selection is based on sample size and shape, T2 and mineralogy. The criteria in are largely based on experience, and may not be exhaustive.

All samples in the project are cylindrical with diameters 38 mm and lengths between 60 mm and 75 mm. This is considered close to optimum for RF coil E. RF coil F may perform acceptably for samples of length up to 110 mm. Sample diameter may increase up to about 60 mm, but at the cost of enhanced image artifacts at the sample margins as the sample extends into areas of greater RF coil inhomogeneity. A cylindrical sample shape is ideal to reduce susceptibility contrast artifacts at the sample margins.

The T2 value of a sample is to a significant extent linked to mineralogy. A sample containing significant amounts of pyrite, magnetite or clay minerals also has a low T2 value, precluding NMR imaging. Small localized concentrations of pyrite or clay minerals may not disturb the general T2 value, but may cause image artifacts around the concentrations.

# IV. Image analysis

**Image analysis tools**
The SISCO NMR scanner is controlled by SISCO's VNMR software running on a Sun workstation. This software is dedicated to control the NMR data acquisition and perform Fourier transformation of the data, but it is not well suited for image analysis. After a 2D Fourier transformation in the VNMR software the image data is therefore transferred to GEUS for further analysis. Data transport is performed by tape files written in SISCO's PHASEFILE format.

The image analysis of NMR data at GEUS is mainly done with the program SISP written in VAX Fortran. It was originally produced by GEUS for use in the JOULE project JOUF-0019, but since then it has been extended several times, e.g. for analysing X-ray CT image data. The key capabilities of SISP are listed below:

1. Input/output facilities in special file formats, e.g. SISCO's PHASEFILE format.
2. Smoothing and filtering facilities.
3. Statistical analysis of image data.
4. Image arithmetic, i.e. pixelwise addition, subtraction, multiplication and division of images.
5. Zoom, translation, mirroring, cut & paste facilities.
6. Image projection and integration facilities.
7. T2 relaxation modeling.
8. Extensible by user delivered subprograms.

**T2 relaxation modeling**
The signal intensities in NMR spin echo images are dependant on several factors. Most of these factors are hardware or system related and may be optimized by proper system setup, i.e. careful RF coil tuning, RF pulse calibration, shimming (homogenization of the static magnetic field B0), pulse programming dedicated to minimize image artifacts, etc. In a technically ideal system, where the system related factors may be disregarded, the intensity variation in a spin echo image is only dependant on **the number of protons in the sample voxels** and **the T1 (spin-lattice) and T2 (spin-spin) relaxation constants of the sample voxels**. The number of protons present in a sample voxel may be correlated to the porosity and fluid saturation of that voxel, which is the focal point of the present project. Therefore, the variation related to T1 and T2 relaxation must be eliminated.

The effects of T1 relaxation are eliminated if the experiment repetition time, TR, is sufficiently long to allow complete T1 relaxation between sample excitation (Kim et al., 1992). In practice complete T1 relaxation is accomplished when TR is above 5 times T1. This condition was adhered to during the project, and the effects of T1 relaxation will not be further considered.

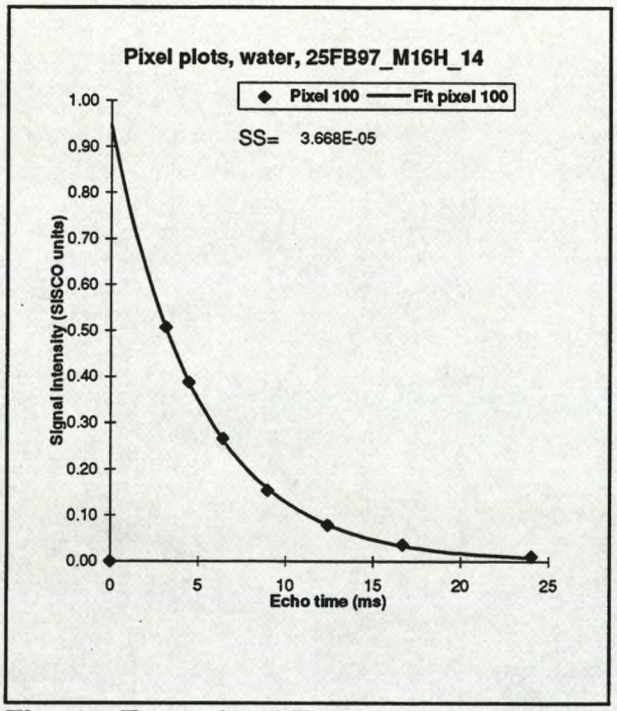


**Fig. 1.** Example of T2 modelization for water in a 1D saturation profile by the TST pulse seauence.

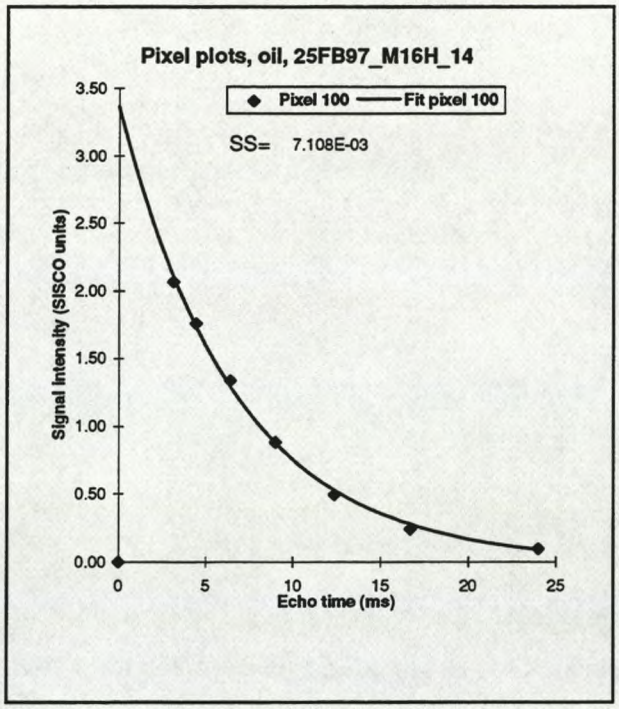


**Fig. 2.** Example of T2 modelization for oil in a 1D saturation profile by the TST pulse sequence.

T2 relaxation is a complex process, covered by a comprehensive literature, for a review see Halperin et al. 1989. T2 relaxation in an inhomogeneous system in principle follows a multiexponential behaviour according to

$$M(t) = \int P(a) \exp[\frac{-t}{T_2(a)}]\, da \qquad (1)$$

where $M(t)$ is the magnetization at time $t$, $P(a)$ is the volume probability density function for pore size $a$, and $T_2(a)$ is the T2 relaxation constant for pores of size $a$ (Halperin et al., 1989).

The T2 relaxation in the sample is compensated by a T2 modelization on a data set of arrayed TE images (Edelstein et al., 1988): An array of images is acquired, that have identical acquisition parameters except for different values of echo time, TE. A T2 modelization is then performed for each image pixel array, producing 2D maps of the fitted parameters, which must include the magnetization at time zero, M0. The TE values of the data acquisition are selected for optimal definition of the signal relaxation. Downwards the setting of TE is restricted by system hardware constraints, i.e. RF power limitations, gradient strength limitations and minimum electronic switching times. Depending on the setup the smallest possible TE value, $TE_{min}$, is presently 2.5 ms in saturation profile experiments (Fig.1 and Fig.2), 6.5 ms in porosity mapping experiments (Fig.3), and 11 ms in saturation mapping experiments (Fig.4 and Fig.5). In arrayed TE experiments the smallest TE value is always selected to be close to $TE_{min}$, in order to trace the relaxation path as close

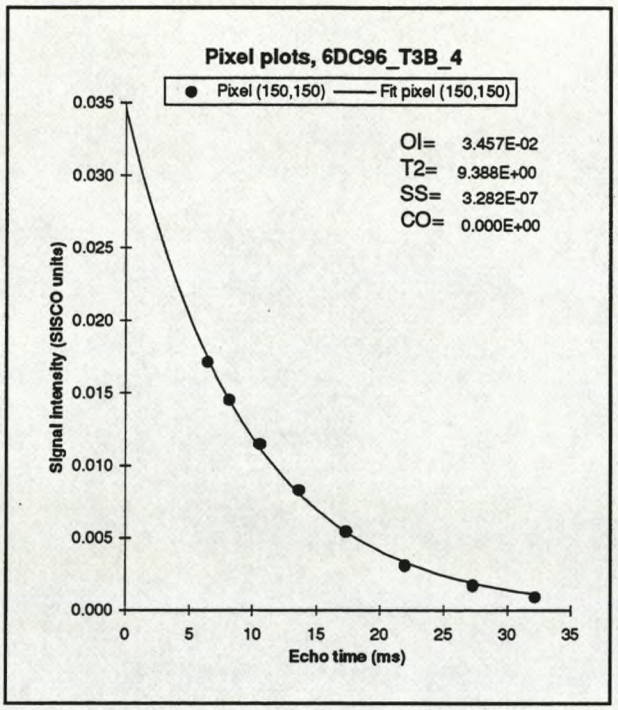


**Fig. 3.** Example of T2 modelization in a 2D porosity map by the SHORTE pulse sequence.

to the M0 value as possible. The largest TE value in an image array is usually selected to be approximately 3 times the anticipated single-exponential T2 relaxation constant, at which time the magnetization M(t) has declined to 5 % of M0 value.

An important issue is the choice of T2 relaxation model. Single-exponential, bi-exponential and stretched exponential modeling were tested by Kim et al. (1992), while Kenyon et al. (1988) tested bi-exponential, tri-exponential and stretched exponential modeling. The conclusion of Kim et al. was that bi-exponential fitting was preferable, while Kenyon et al. found that stretched exponential fitting was preferable. The present project has repeatedly tested single-exponential fitting and stretched-exponential fitting, and finds that although stretched exponential fitting clearly produce the best fits in terms of statistical measures like mean square of deviates (MSD), M0 is more

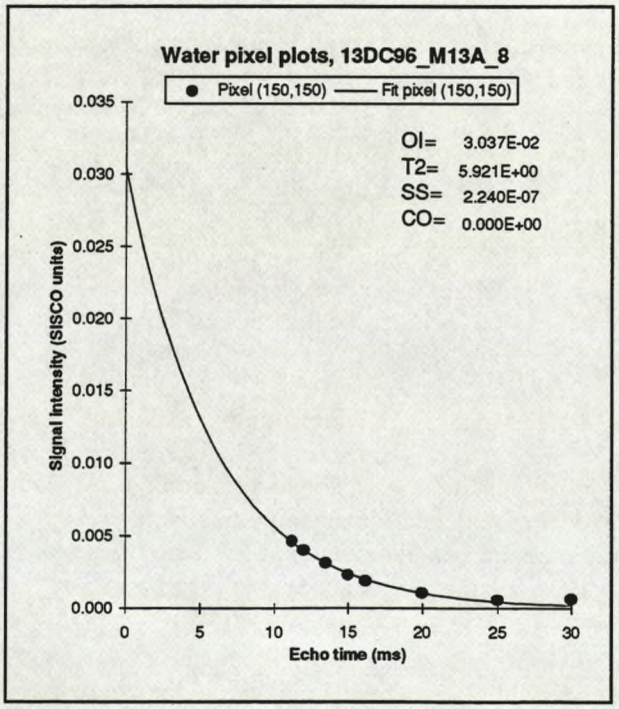


**Fig. 4.** Example of a T2 modelization for water in a 2D saturation map by the CSI2D pulse sequence.

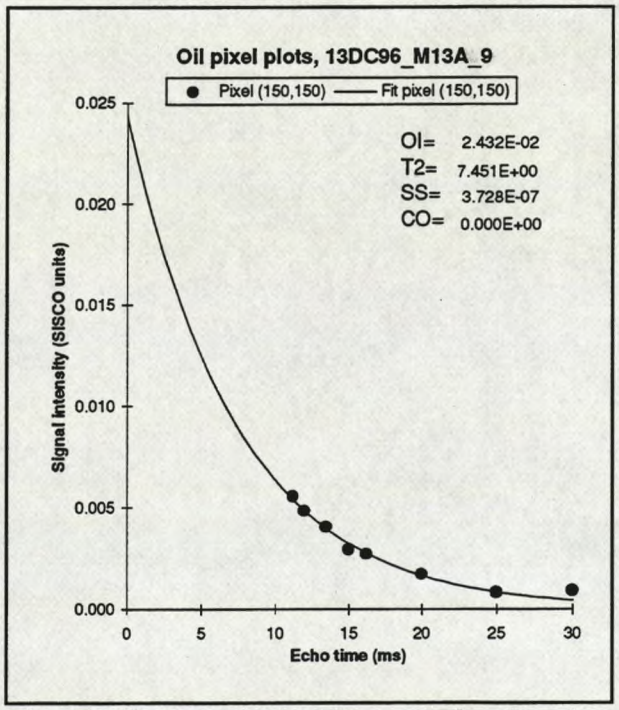


**Fig. 5.** Example of a T2 modelization for oil in a 2D saturation map by the CSI2D pulse sequence.

confidently determined by single-exponential fitting. This apparent discrepancy stems from the non-linear nature of the modeling and the fact that M0 is determined by a significant extrapolation outside the sampled data interval, cf. Figs. 1 to 5.

Examples of T2 relaxation models are presented in Figs. 1 to 5. The figures present models for representative pixels in the three imaging methods covered by this work. The small $TE_{min}$ of the saturation profile experiment (Fig.1 and 2) ensures a fairly short extrapolation along the model function to obtain the M0 value. The precision of the M0 determination is consequently good, and so is the saturation determined from the data. In the saturation map experiment (Figs.4 and 5), on the contrary, the large $TE_{min}$ requires a long extrapolation along the model function to obtain the M0 value, and the precision of the determination is much inferior to the saturation profile method. Lack of pixelwise precision may to some extent be alleviated by filtering, but at the cost of reduced spatial resolution. The porosity map experiment (Fig.3) is intermediate between the other two methods in precision.

# V. 2D porosity determination

The 2D porosity determination method is based on the spin echo pulse sequence of Edelstein et al. (1980). In the SISCO implementation this pulse sequence is named SHORTE, and the echo is generated by a 180° pulse, rather than by reversing the read-out gradient as in the original version of the pulse sequence.

The maps presented in this chapter are based on 256 x 256 pixel images.

**Sample considerations**
The sample should have an acceptable T2 relaxation constant. Ideally the T2 value should be as long as possible. Good porosity images have been produced on samples with T2 values down to 8.2 ms (sample M15B). It is estimated that reasonable porosity maps could be produced on samples with T2 values down to 5 ms. This implies that porosity maps can be produced on most Maastrichtian chalk samples, while Danian and pre-Maastrichtian chalk samples are mainly excluded. Clean sandstone samples have T2 values in the acceptable range, but porosity mapping has not been attempted.

**Pore fluid considerations**
The SHORTE pulse sequence is not capable of selectively selecting the signal from water or oil. The detected signal is the combined signal from all fluids present in the sample. Because different fluids have different proton densities, converting signal intensities to fluid amounts is impossible when more than one fluid is present. An additional complication is that the signal from oil is shifted relative to the signal from water along the read-out direction by an amount equal to

$$L = \frac{2*\pi * \Delta_{chemical\ shift}}{\gamma * G_{read\text{-}out}} \qquad (2)$$

where $L$ is the size of the shift, $\Delta_{chemical\ shift}$ is the size of the chemical shift separation, $\gamma$ is the gyromagnetic ratio for $^1H$, and $G_{read\text{-}out}$ is the size of the read-out gradient. Eq.2 predicts a shift of approximately 4 mm for a typical experimental setup.

The problems are avoided by saturating the sample with a single suitable fluid. Most samples in this study were saturated with water containing 1.0 weight-% NaCl and 0.005 mol/l $Ni(NO_3)_2$. This fluid is called NMR-1 brine. The Ni content results in rapid T1 relaxation allowing fast data acquisition, while the NaCl content assures a reasonable loading of the RF coil. The choice of fluid is important, see below under the example of M15B for a discussion of coil loading.

To avoid liberation of a separate gas phase within the pore space of the sample the

pore fluid is degassed. Voxels containing a free gas phase will have an erroneously low porosity in the final 2D map.

**Procedure for 2D porosity mapping**
The following two procedures have been tested for the generation of 2D porosity maps from a suitable sample.

Procedure 1:

1. Measurement of sample bulk porosity, $\Phi$.
2. Saturating the whole pore space of the sample with a suitable fluid.
3. Mounting the sample in the NMR scanner in a suitable RF coil.
4. Acquisition of NMR data resulting in an array of images with different echo times, TE.
5. Data processing by program SISP:
   A. Filtering of image data, if necessary.
   B. T2 modelization of the image array to calculate an M0 map for the sample.
   D. Calculation of the mean value in the M0 map, mean{M0}.
   E. Pixelwise multiplication of M0 by $\Phi$/mean{M0} to convert M0 to a **porosity map**.

Procedure 2:

1. Measurement of sample bulk porosity, $\Phi$.
2. Saturating the whole pore space of the sample with a suitable fluid.
3. Mounting the sample in the NMR scanner in a suitable RF coil at a known position. The same position must be used for the coil homogeneity phantom (Step 5).
4. Acquisition of NMR data resulting in an array of images with different echo times, TE.
5. Repeating Step 3 and Step 4 with the coil homogeneity phantom.
6. Data processing by program SISP:
   A. Filtering of image data, if necessary.
   B. T2 modelization of the two image arrays to calculate M0 maps for both the sample, $M0_{sample}$ and the coil homogeneity phantom, $M0_{phantom}$.
   C. Pixelwise division of the $M0_{sample}$ map by the $M0_{phantom}$ map to correct for RF coil inhomogeneity. The new map is termed $M0_{sample,corr}$.
   D. Calculation of the mean value in $M0_{sample,corr}$, mean{$M0_{sample,corr}$}.
   E. Pixelwise multiplication of $M0_{sample,corr}$ by $\Phi$/mean{$M0_{sample,corr}$} to convert $M0_{corr}$ to a **porosity map**.

Remark that both procedures force the mean porosity in the map to equal the externally determined value of $\Phi$. Attempts have been made to produce porosity maps solely from signal intensities, without the data normalization steps 4D and 4E. In these attempts the sample signal was scaled with the signal from a phantom of known proton density. The attempts were unsuccessful as the calculated mean porosities of samples deviated as much as 7 % from porosities determined by conventional core analysis. The failure probably stems from unaccounted coil

loading effects, see discussion under sample M15B.

**RF coil inhomogeneity effects: Sample M15B**

Sample M15B consists of chalk of Maastrichtian age from the Dan field. The sample is cylindrical with diameter 38 mm and length 71 mm. The sample is traversed by a stylolite zone at an angle of approximately 45° to the cylinder axis. Prior to NMR analysis the bulk porosity was measured to be 0.334 (Φ-fraction) by the He-injection method. The pore fluid at the time of NMR measurement was water with 0.005 mol/l $Ni(NO_3)_2$. The image slice contains the cylinder axis, and makes an angle of approximately 20° to the normal of the stylolite plane. The thickness of the image slice is 3.5 mm, which means that the image slice contains 12 % of the total volume of the sample.

For comparison the sample has been analysed by both Procedure 1 and Procedure 2.

Fig.6 is the porosity map resulting from Procedure 1. The stylolite zone is prominent in the lower half of the map, showing pixel porosities values with a variation significantly above the sample mean. An indistinct layering is visible at an angle of approximately 35° to the length of the sample, and an angle of approximately 100° to the stylolite zone. It is coincident with one of the two main directions of healed hairlines in the sample. The other main hairline fracture direction lies approximately in the image slice, and is therefor not visible. The standard deviation (1σ) of the porosity values within the sample is 0.027 Φ-fraction.

Fig.7 is the porosity map resulting from Procedure 2. The M0 map of the phantom DPH1 used to correct for coil inhomogeneity is shown in Fig.8. The porosity map in Fig.7 displays the same lithological structures as Fig.6. In addition the map displays an increased porosity gradient between the margin and centre of the sample. The standard deviation (1σ) of the porosity values within the sample is 0.032 Φ-fraction, which is significantly higher that in Fig.6. This indicates that an artificial variability has been added to the map by the coil inhomogeneity correction of Procedure 2. It is therefore concluded that coil inhomogeneity **is not** adequately compensated by Procedure 2.

The signal inhomogeneity in phantom DPH1 (Fig.8) is large compared to the expected variation, with a coefficient of variation, $S.D./X_{mean}$, of 0.051. For comparison, the coefficient of variation of the uncorrected M15B porosity map (Fig.6) is 0.081. Repeated measurements on the sample reveal similar distributions. The reason for the large signal inhomogeneity in images of fluid phantoms is only partly known. It is suggested to be related to the phenomenon of **coil loading**. It is well known that the excitation efficiency of an RF coil is dependant on the intensity of eddy currents in the medium contained in the coil. Higher intensity of eddy current results in lower excitation efficiency. The intensity of eddy currents is proportional to the size and conductivity of the medium inside the coil. In the instance of M15B and DPH1 the latter contains a much larger amount of conducting medium, and the medium also has a considerably higher conductivity. This results in a much higher coil loading by phantom DPH1 relative to sample M15B. The

unexpectedly large signal inhomogeneity in the case of phantom DPH1 may result if the **variation** of excitation efficiency is also affected by coil loading, i.e. if the distribution of flip angles of RF pulses in the coil varies with coil loading.

If the hypothesis is correct, Procedure 2 may work as expected if the coil loading of the phantom is matched to the sample. This can be accomplished by simply reducing the salinity of the brine in the phantom. The effects of possible non-linearity in the data acquisition system can be reduced by diluting the $^1H_2O$ content of the phantom with $^2H_2O$ to match the proton density of the sample. Until these possibilities have been tested Procedure 1 is recommended as the best procedure for production of porosity maps.

**Reproducibility of porosity map**

Sample T3B is a sample of Maastrichtian chalk from the Tyra field. The bulk porosity is 0.462 Φ-fraction. The sample is cylindrical with diameter 38 mm and length 70 mm. Two runs on sample T3B were performed on November 1st, 1996 and December 6th, 1996 for reproducibility testing. The experiment setups were as identical as possible, i.e. using same RF coil, shimming procedure, pulse calibration procedure, pulse sequence and acquisition parameters. The thickness of the image slice is 4.0 mm for both acquisitions. The image slice contains the cylinder axis. The image plane is parallel to the sample layering. Procedure 1 was used for calculating the porosity maps presented in Figs.9 and 10. The standard deviation ($1\sigma$) of the porosity values is 0.033 Φ-fraction in Fig.9 and 0.031 Φ-fraction in Fig.10.

Both maps reveal a complicated pattern of crisscrossing sublinear zones of width 1 to 2 mm. The porosity values of the zones are 0.02 to 0.05 Φ-fraction below the sample mean. The zones are healed hairline fractures. Several features with porosity values 0.05 to 0.15 Φ-fraction below sample mean are not readily interpreted, but may be caused by trace fossils or cemented features.

The difference between the two maps is illustrated with Fig.11, which is a map of the pixelwise difference between Fig.9 and Fig.10. Fig.11 shows that in the major part of the image slice Fig.9 and Fig.10 differs by less than 0.02 Φ-fraction. In an area along the central and lower left sample margin and in the lower right corner of the sample the difference between the two maps is larger. The standard deviation of the porosity difference values in Fig.11 is 0.028 Φ-fraction, which is a measure of the reproducibility of the porosity mapping. This value includes both the error in repositioning the sample in the second analysis and the analytical error. The error in sample positioning is mainly connected with the angular adjustment of the cylindrical sample, which at present is only done by eye. The analytical error, i.e. deviation between measured and true porosity value, is estimated to be below 0.02 Φ-fraction.

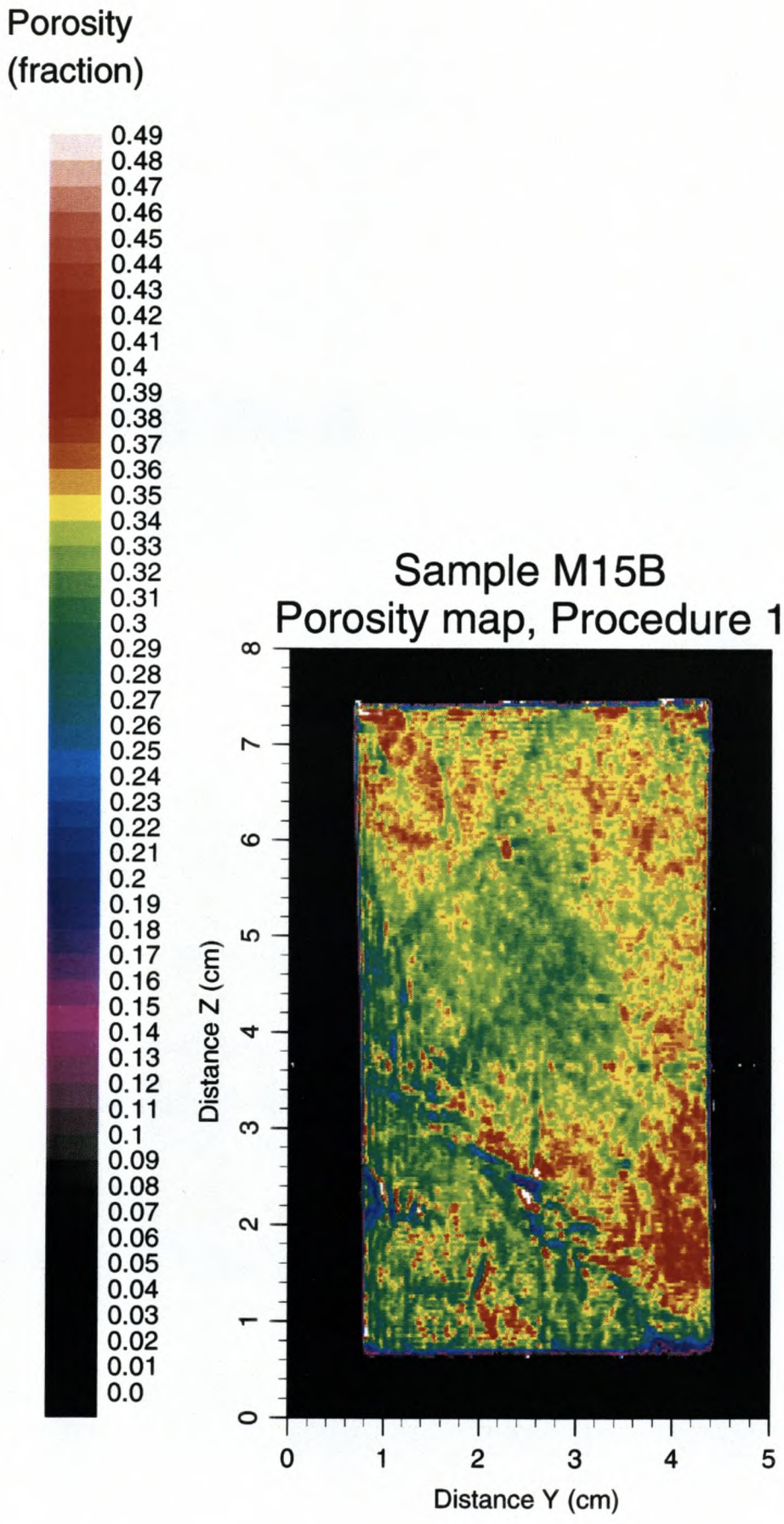


Fig. 6

Fil efj2upo1, 15-Apr-97, kl. 10:20:25

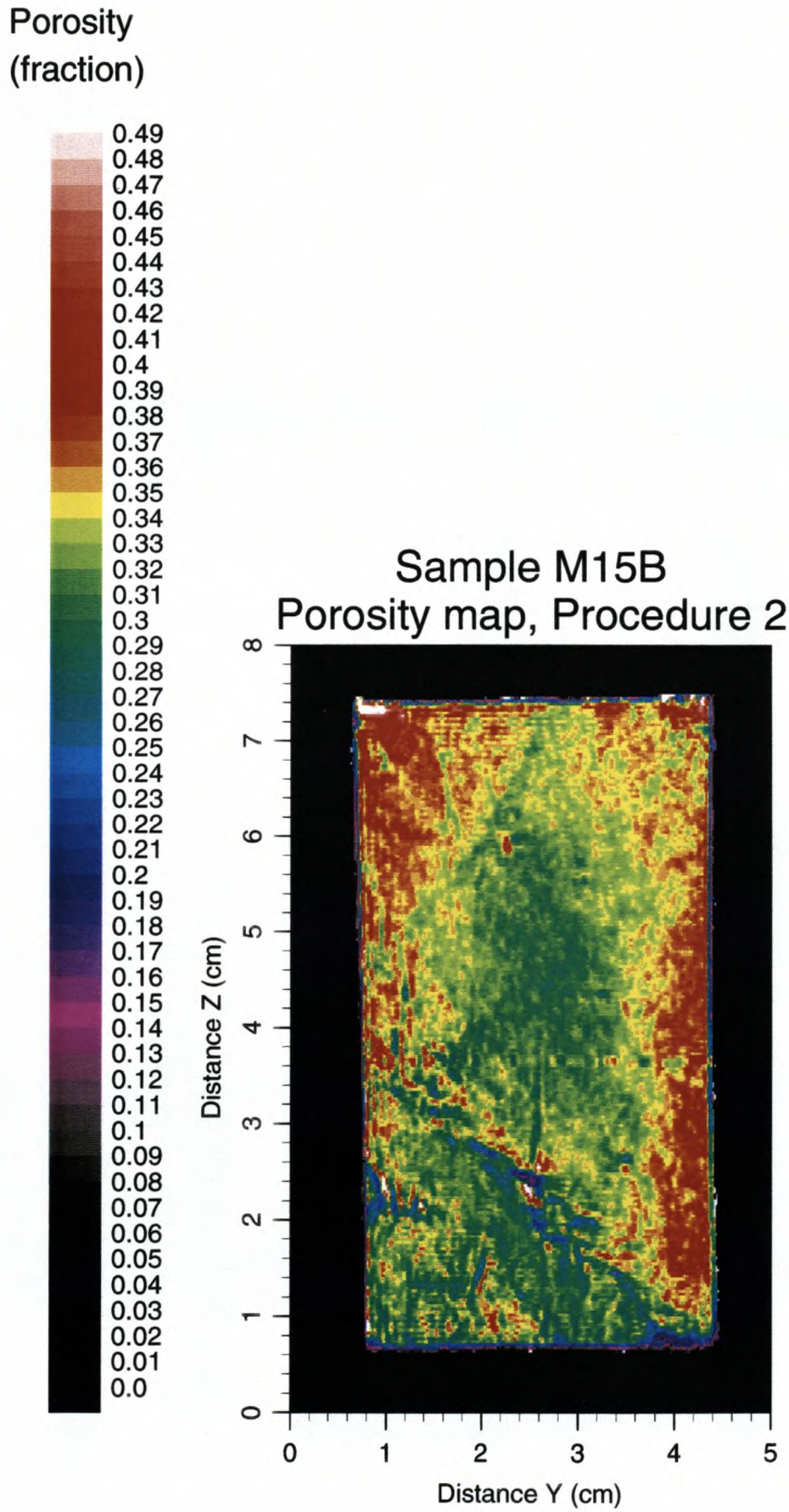


Fig. 7

Fil efj2upo3, 15-Apr-97, kl. 10:17:57

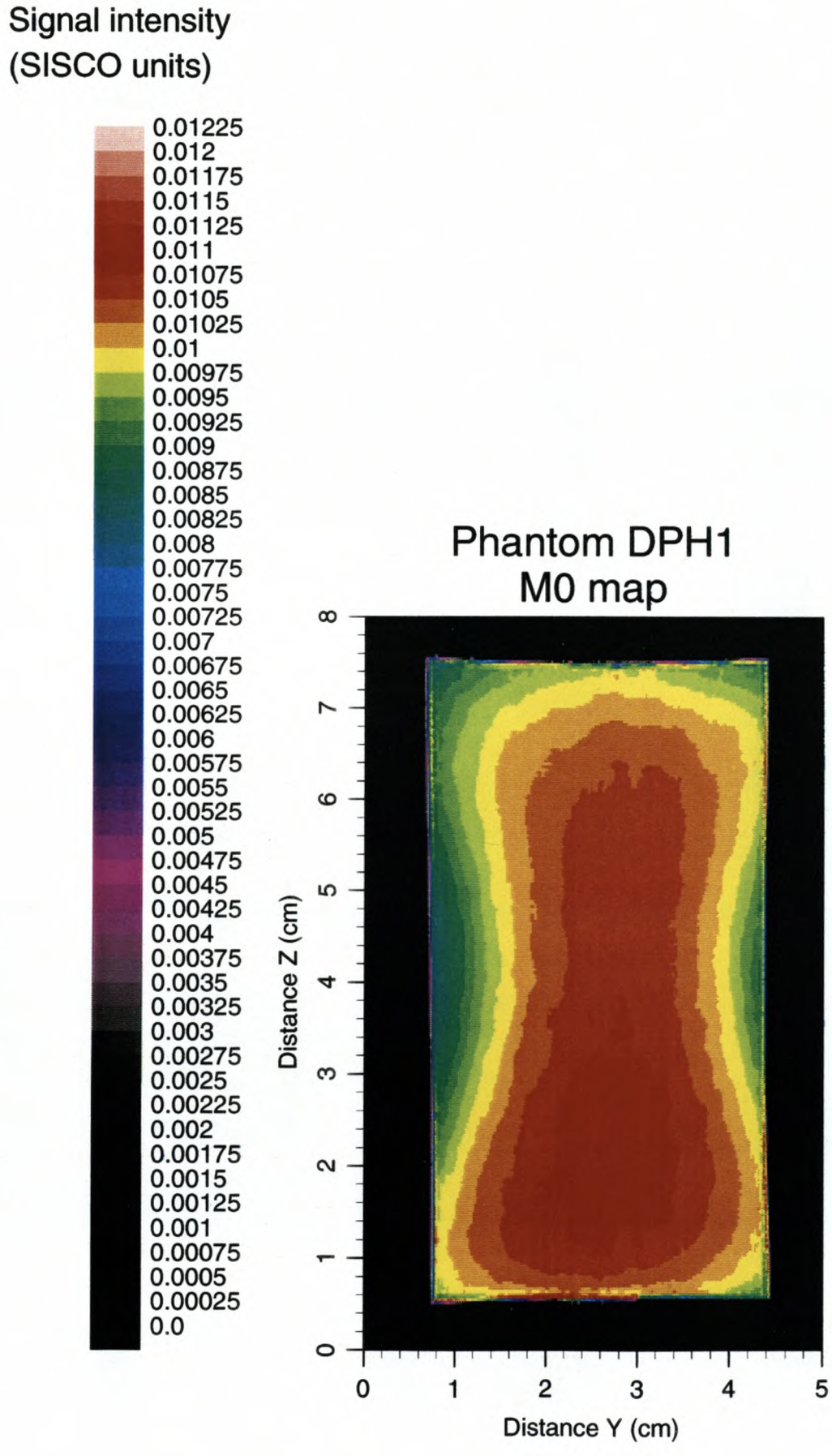


Fig. 8

Fil dphl2oidb, 15-Apr-97, kl. 09:48:33

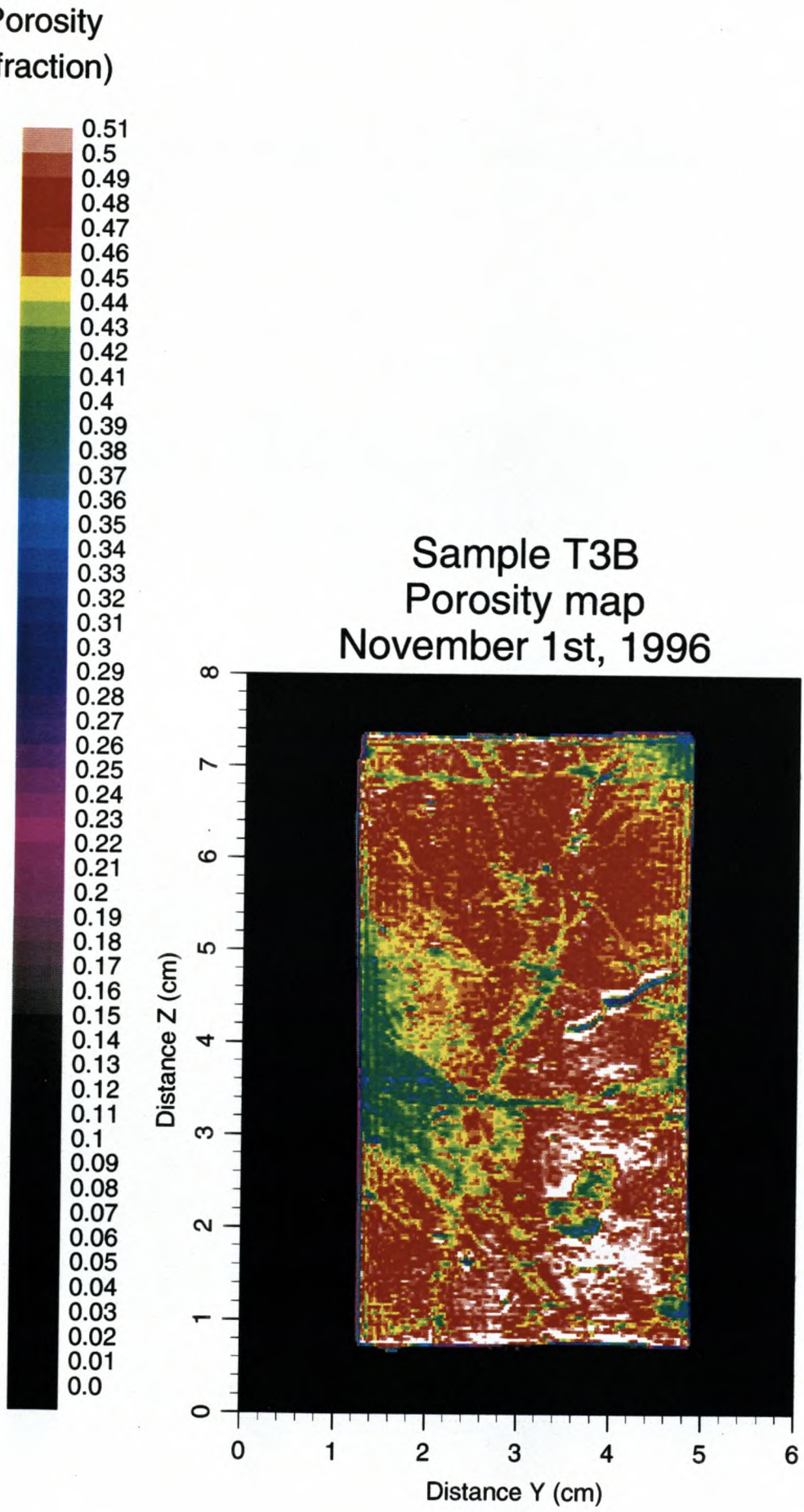


Fig. 9

Fil efb93po, 15-Apr-97, kl. 10:39:36

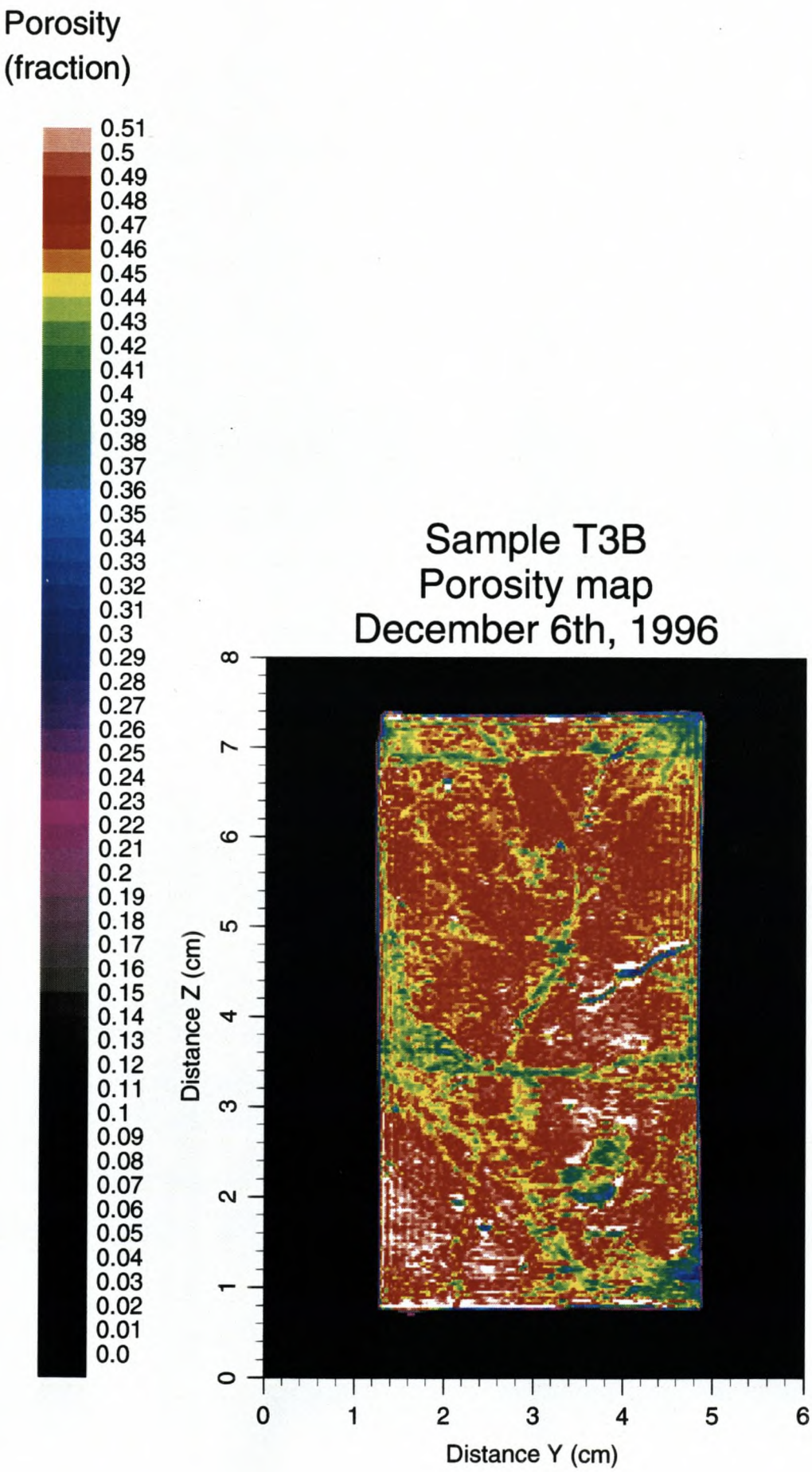


Fig. 10

Fil eff41po, 15-Apr-97, kl. 10:42:15

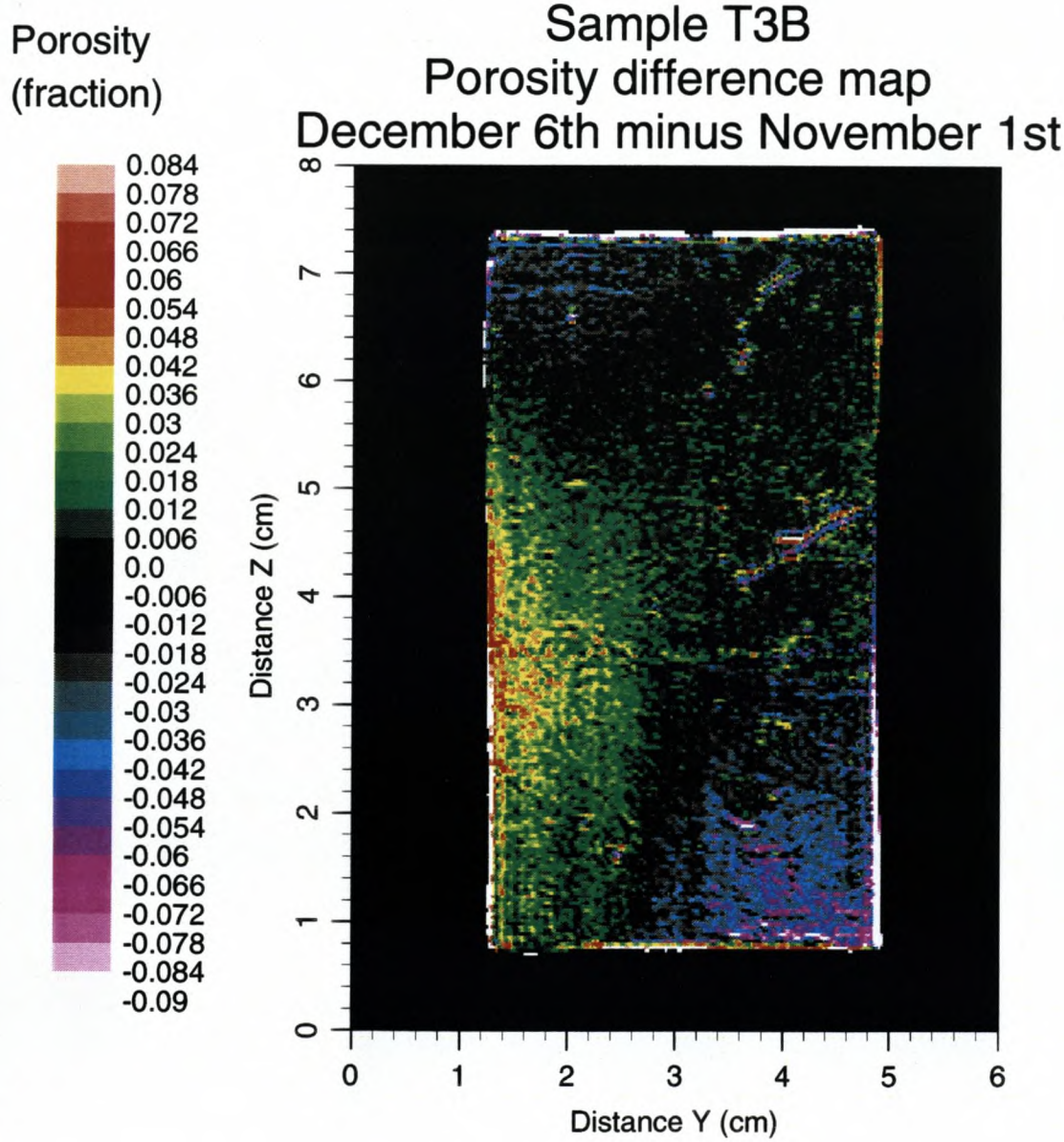


Fig. 11

Fil t3bpodif, 15-Apr-97, kl. 10:44:53

# VI. 1D saturation determination

In an EFP-93 project (ENS J.no. 1313/93-0014) an NMR method for quantitative determination of 1D saturation profiles was developed (Olsen et al., 1996). This method has proved quite useful for investigating fluid distributions in core samples, especially in combination with core flooding experiments. The method is currently the fundamental laboratory method in the EFP-96 project "Saturation functions and wettability in chalk" (ENS J.no. 1313/96-0005).

Within the present project the NMR 1D saturation profile method is evaluated together with a $\gamma$-transmission method employed at Physics Department and Department of Automation, an electrical impedance method employed at Department of Chemistry, and an X-ray CT method employed at Department of Chemical Engineering. The comparison of the methods will appear in the final report of the project.

**Improvement of pulse sequence TST**

The pulse sequence of the 1D saturation determination method, TST, has been significantly improved during the project. In the original version of the pulse sequence (Olsen et al., 1996) the signal is acquired as a symmetric echo. This is the standard technique in most imaging pulse sequences because it assures maximum spatial resolution in the read-out direction, and it presents no TE related problems when echo time considerations are not important. In the case of geological material echo time considerations become paramount, and resolution is less important. Resolution in the case of the TST pulse sequence means frequency resolution as read-out gradients are absent from the pulse sequence. In the improved version of the TST pulse sequence the user is free to select any acquisition form along the continuum from full symmetric echo acquisition to half echo acquisition. In practice it seems that a highly asymmetric echo with echo time around 3 ms works very well, cf. Figs. 1 and 2. The abandonment of symmetric echo acquisition enables extension of signal acquisition as far as desired, which significantly reduces previous image artifacts resulting from Fourier transforming a sharply truncated signal. The cost of the reduced $TE_{min}$ is a slightly reduced frequency resolution. In a large majority of the analysed samples, the spectral peaks are well resolved and a slight loss of resolution is unimportant.

The TST saturation profiles presented in this chapter are measured with the old version of the TST pulse sequence, because the improved version only became operative in December 1996. However, the improved version has been used successfully by the EFP-96 project mentioned above in February 1997. The pixel plots of Figs. 1 and 2 originate from the improved version.

**Saturation profiles for comparison with other physical methods**
1D saturation profiles were measured with the TST pulse sequence on two samples, M721 and M13A, in comparison sessions with the other physical methods addressed by the project. All profiles contain 256 pixels.

Sample M721 is a sample of Maastrichtian chalk, cf. Table I for sample data. The porosity value is the mean of a determination before the comparison session and a determination after the session. The sample was prepared by GEUS and was circulated first to Department of Automation for $\gamma$-transmission measurement, then to Department of Chemical Engineering for CT-scanning, and finally to GEUS for NMR measurement. Sample preparation consisted of plugging a 1.5" plug sample, cleaning the sample, conventional core analysis, saturating the sample with brine, and finally flooding the sample with n-decane at a constant flow rate of 10 ml/h. During the comparison session an oil flow of 10 ml/h was sustained all the time by use of a Mobile Flooding Unit (Nørgaard et al., 1995). This preparation procedure generated and sustained a pronounced capillary end effect during the whole comparison session. The preparation procedure was developed by the above-mentioned EFP-93 project (Nørgaard et al., 1995). After the comparison session the bulk fluid saturation of the sample was verified by Dean Stark analysis at GEUS. The Dean Stark analysis was in close agreement with a bulk fluid saturation determination by NMR technique, cf. Table I. Please remark that the NMR technique constrains $S_w+S_o$ to equal 100 %. The technique therefore requires the sample to be gas free. The Dean Stark analysis demonstrates that this was the case.

The TST fluid saturation profile measured on sample M721 is presented in Fig.12. The profile reveals a pronounced capillary end effect with $S_w$ reaching 69 % at the sample outlet. Sample M721 is a vertical plug with two transverse stylolites and a distinct lamination. The major irregularities of the saturation profile are likely to be caused by these lithological structures. During acquisition of the saturation profile sample M721 was enclosed in a Hassler core holder. A small fluid amount was present in the end fittings of the core holder, giving rise to a measurable signal at each end of the sample proper. The position of these signals is indicated in Fig.12.

Like sample M721, sample M13A is a sample of Maastrichtian chalk, cf. Table II for sample data. The porosity value is the mean of a determination before the comparison session and a determination after the session. The sample was prepared by GEUS. After an initial NMR measurement at GEUS, the sample was circulated between Department of Automation and Department of Chemical Engineering for several measurements by $\gamma$-transmission and X-ray CT-scanning. It was finally returned to GEUS for a final NMR measurement. Sample preparation consisted of plugging a 1.5" plug sample, sample cleaning, conventional core analysis, saturating the sample with brine, and flooding a limited amount of n-decane into the sample. Unlike sample M721 oil flow was not sustained during the comparison session. Injection of n-decane into the sample was stopped well before breakthrough, and the downstream end of the sample therefore contained a water saturation of 100 %. For protection against evaporation the sample was wrapped in saran foil during measurement, and it was stored in n-decane when measurement

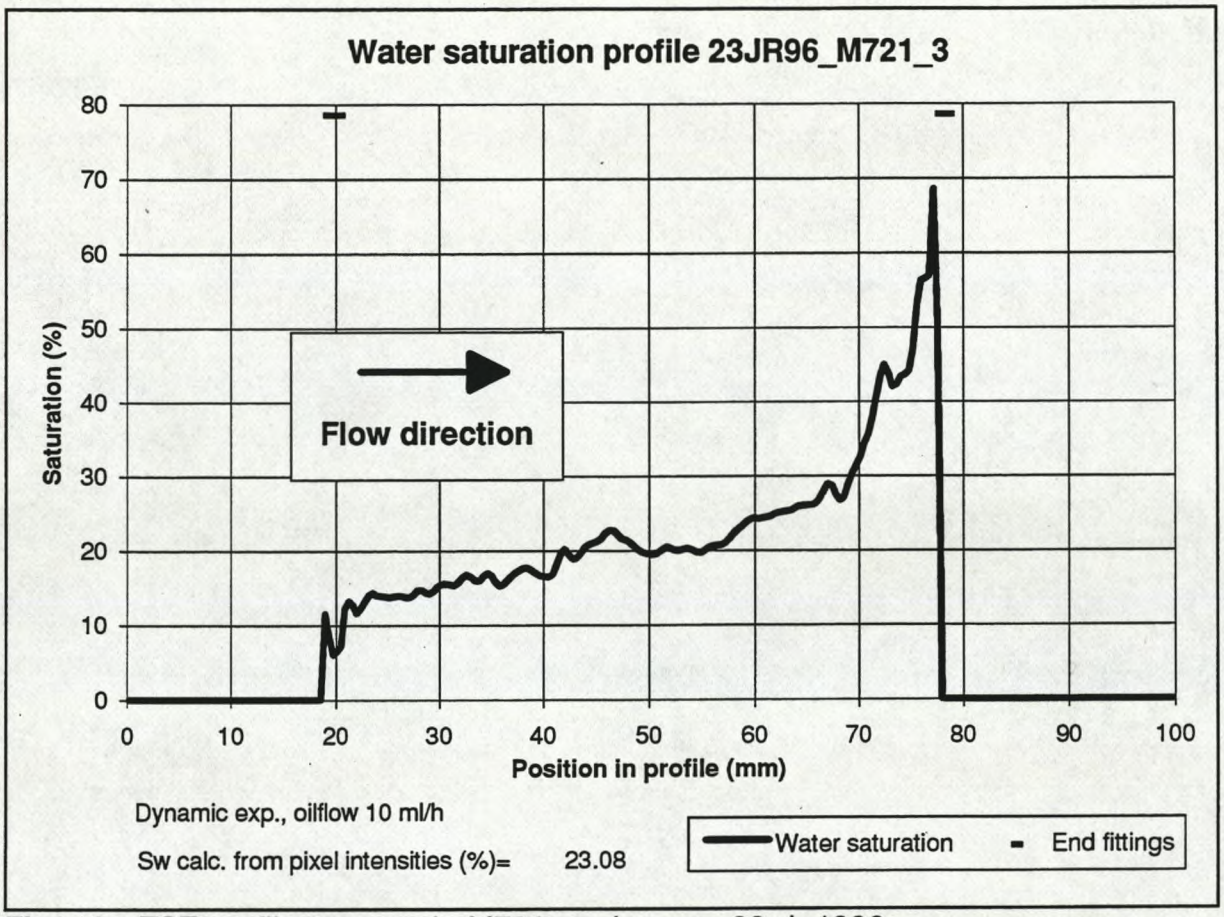


**Fig. 12.** TST profile on sample M721 on January 23rd, 1996.

**TABLE I.** Sample M721 data sheet

| | |
|---|---|
| Well: | Dan MFB-7 |
| Length (mm): | 62 |
| Diameter (mm): | 38 |
| Porosity (%) | 29.1 |
| Liquid permeability (mD) | 0.80 |
| Dean Stark bulk saturation determination after NMR measurement: | |
| $S_w$ (%):<br>$S_o$ (%):<br>$S_g$ (%): | 23.9<br>75.8<br>0.4 |
| NMR TST bulk saturation determination: | |
| $S_w$ (%):<br>$S_o$ (%): | 23.08<br>76.92 |

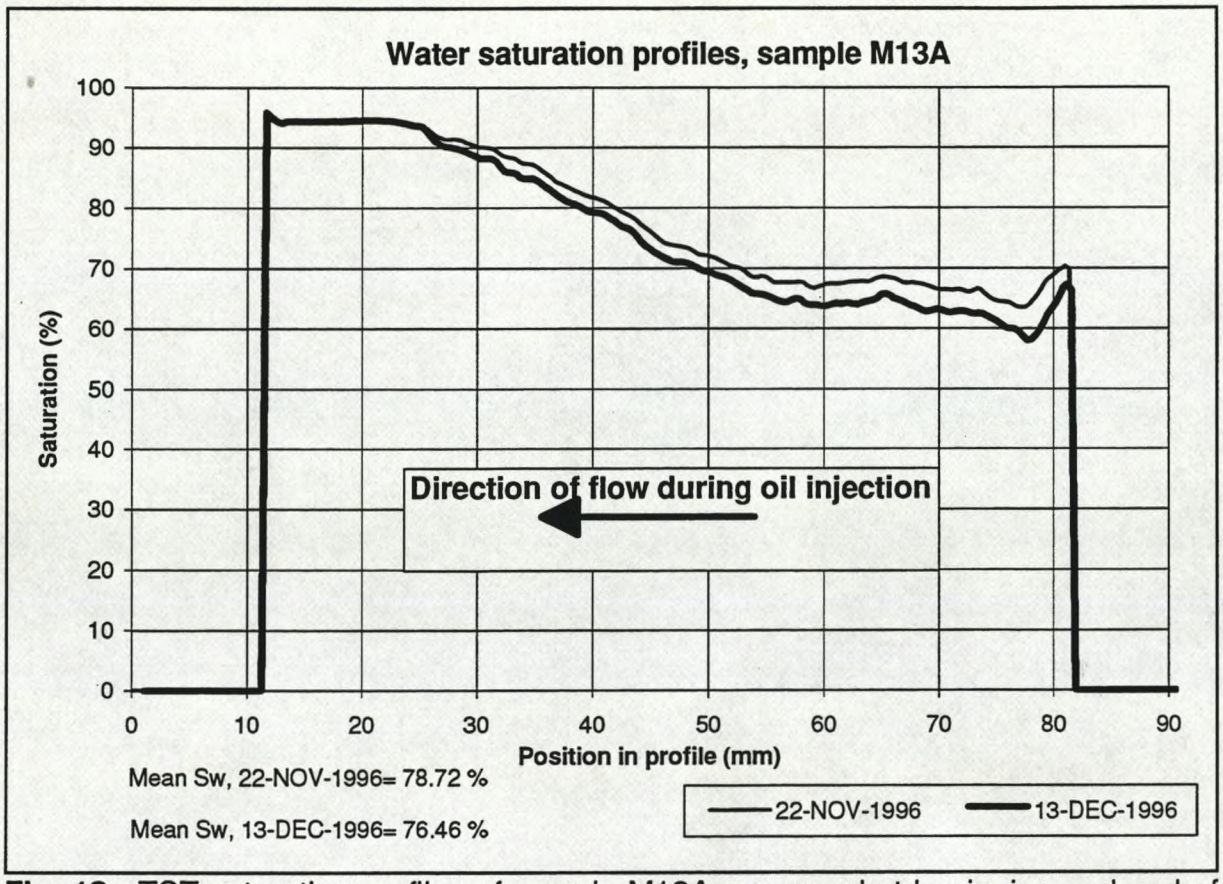


**Fig. 13.** TST saturation profiles of sample M13A measured at beginning and end of physical method comparison session.

**TABLE II.** Sample M13A data sheet.

| | |
|---|---|
| Well: | Dan MFB-13 |
| Length (mm): | 74 |
| Diameter (mm): | 38 |
| Porosity (%) | 28.4 |
| Liquid permeability (mD) | 0.72 |
| Gravimetric bulk saturation determination before NMR measurement: | |
| $S_w$ (%):<br>$S_o$ (%): | 78.9<br>21.1 |
| NMR TST bulk saturation determination 22.November 1996: | |
| $S_w$ (%):<br>$S_o$ (%): | 78.7<br>21.3 |
| NMR TST bulk saturation determination 13.December 1996: | |
| $S_w$ (%):<br>$S_o$ (%): | 76.5<br>23.5 |

was not in progress. Before the comparison session the bulk fluid saturation of the sample was verified by gravimetry. The gravimetric result is in close agreement with a bulk fluid saturation determination by NMR technique at the start of the comparison session, cf. Table II. Please remark that both the NMR and the gravimetric techniques constrain $S_w+S_o$ to equal 100 %.

The TST fluid saturation profiles measured on sample M13A are presented in Fig.13. The profiles reveal a significant saturation gradient. Close to the outlet end of the sample the two saturation profiles converge at an $S_w$ value of 95 %. This disagrees with the known water saturation of 100 % in the outlet end of the sample. The disagreement is caused by interference between the water and oil NMR signals. The effect of the interference on the calculated fluid saturations is proportional to the dissimilarity in strength between the water and oil signal: When the signals differ significantly in strength the smaller signal is significantly increased by the interference, while the interferences largely cancel out when the signals are of approximately equal strength.

The two water saturation profiles of Fig.13 are in good agreement, but the $S_w$ values in the December 13th profile is consistently below the $S_w$ values in the November 22nd profile. The mean $S_w$ deviates by 2.2 %, which is equivalent to 0.5 ml of water when the pore volume of the sample is considered. The decrease in $S_w$ may by caused by a minor evaporation from the sample, or it may be an analytical error. A decrease in $S_w$ is also shown in NMR bulk spectra from November 22nd and December 13th, and a 2D saturation map on December 13th shows signs of evaporation (Fig.15). It is therefore considered unlikely that the difference between the saturation profiles is caused by analytical error.

Sample M13B contains a distinct oblique lamination. On December 13th the sample was also analysed by the 2D fluid saturation method, cf. Chapter VII.

The accuracy of the pixel fluid saturations in the 1D saturation profiles is considered to be 5 % (Olsen et al., 1996), while the reproducibility is 2 %.

# VII. 2D saturation determination

The 2D saturation determination method, like the 2D porosity determination method, is based on the spin echo pulse sequence of Edelstein et al. (1980). In the SISCO implementation the pulse sequence, named CSI2D, is modified to include chemical shift selection capabilities, by removing slice selection gradients from the excitation pulse interval, and by using a frequency selective gauss-shaped pulse for excitation. The cost of the chemical shift selection capability, relative to the SHORTE pulse sequence, is an increase in minimum echo time, $TE_{min}$, of 3 ms.

**Experiment considerations**
Separate images of the distribution of water and oil in the sample are obtained by running the CSI2D pulse sequence twice with identical setups, except for setting the RF frequency at the water resonance frequency resp. the oil resonance frequency. The length of the excitation pulse is selected to excite only the target fluid, i.e. water or oil in the sample. This method requires that the water and oil signals are well separated in the frequency spectrum. This is the case for all investigated Maastrichtian chalk samples, where the water and oil signals are separated by 700 to 800 Hz, while the Full Width at Half Maximum (FWHM) of the peaks ranges from 60 to 230 Hz. Another requirement of the method is that the target fluid has constant resonance frequency in the whole sample. In all Maastrichtian samples this has been accomplished by careful shimming.

Both water and oil acquisitions are performed as arrayed acquisitions with the number of images in each acquisition ranging from 4 to 8. Using the image analysis program SISP a T2 modelization is performed on both the water image array and the oil image array, resulting in two M0 maps, $\mathbf{M0_{water}}$, and $\mathbf{M0_{oil}}$. These maps give the distribution of magnetization at time zero attributable to water protons resp. oil protons. Disregarding RF coil inhomogeneity effects, the pixel values in the magnetization maps are proportional to the number of water protons resp. oil protons in the corresponding sample voxels. So, the M0 maps are **proton concentration** maps. Fluid saturation in a rock sample, however, is defined as the **volume ratio** of fluids in the sample pores. It is therefore necessary to convert the proton concentrations of the M0 maps to volume fractions. This is done by dividing the pixel proton concentration values by the proton densities of the respective fluids. Proton density is defined as the number of protons per unit volume. It may be measured on a fluid sample, but is more accurately calculated from a chemical analysis. Correcting $M0_{water}$ and $M0_{oil}$ for proton density results in two new maps, $\mathbf{M0_{water,\ corr\ PD}}$ and $\mathbf{M0_{oil,\ corr\ PD}}$. The fluid saturation maps for water, $\mathbf{FS_{water}}$, and oil, $\mathbf{FS_{oil}}$, now may be calculated as

$$FS_{water} = \frac{M0_{water,corrPD}}{M0_{water,corrPD} + M0_{oil,corrPD}} \quad (3)$$

$$FS_{oil} = \frac{M0_{oil,corrPD}}{M0_{water,corrPD} + M0_{oil,corrPD}} \quad (4)$$

It is recognized that this method forces $FS_{water} + FS_{oil}$ to equal 1.0 in every pixel. All information in one map is therefore also contained in the other map. Nonetheless, plotting both $FS_{water}$ and $FS_{oil}$ is often advantageous as the colour scales of the maps may highlight different features in the maps, cf. Figs. 14 and 15.

A requirement for reliable results is that the sample does not contain a free gas phase. Voxels with a free gas phase will produce less signal than voxels without a free gas phase, but as Eq. 3 and 4 forces the total saturation to equal 1.0, the saturations $S_w$ and $S_o$ for gas containing voxels will be erroneously high. The **ratio** between $S_w$ and $S_o$ will be correct in all instances.

A major advantage of the method is that is self-correcting with respect to RF coil inhomogeneity. Any magnetization anomalies in the M0 maps caused by RF coil inhomogeneity will be equally distributed in $M0_{water}$ and $M0_{oil}$, and will consequently cancel out in Eqs. 3 and 4. A major disadvantage of the method is the high minimum echo time, $TE_{min}$, of 11 ms, cf. Figs. 4 and 5 and discussion in Chapter IV.

**Procedure for 2D saturation mapping**

The generation of a 2D saturation map from a suitable sample includes the following steps. The sample should contain a mixture of water and oil with a minimum of free gas.

1. Mounting the sample in the NMR scanner in a suitable RF coil.
2. Acquisition of NMR data. The water and oil signals are sampled in two separate arrays of images. The images of each array are identical except for echo time, TE.
3. Data processing by program SISP:
   A. Filtering of image data, if necessary.
   B. T2 modelization of the two image arrays to calculate M0 maps, $M0_{water}$ and $M0_{oil}$ for the water and oil signals.
   C. Correction for proton density by dividing every pixel in $M0_{water}$ with $PD_{water}$ to produce $M0_{water,\ corr\ PD}$, and by dividing every pixel in $M0_{oil}$ with $PD_{oil}$ to produce $M0_{oil,\ corr\ PD}$.
   D. Calculation of fluid saturation images $FS_{water}$ and $FS_{oil}$ according to Eqs. 2 and 3.

**Example of a 2D saturation map: Sample M13A**

Sample M13A is a sample of Maastrichtian chalk that was also used for developing the 1D saturation profile method, cf. Chapter VI. Sample data is presented in Table II. The sample contains a distinct oblique layering, but no stylolites. The sample was prepared for analysis by injecting a limited amount of n-decane into a

brine saturated sample. Injection was stopped well before breakthrough to assure that the downstream end of the sample had an $S_w$ equal to 100 %. The NMR data was acquired while the sample was wrapped in saran foil for evaporation control. Refer to Chapter VI for full details of sample preparation.

A 2D water saturation map is presented in Fig.14 and a 2D oil saturation map in Fig.15. The maps are based on 256 x 256 pixel images. As the maps contain the same information, the following description applies to both maps.

The lamination of the sample is distinctly seen as layers of contrasting saturation with an angle of 50° to the cylinder axis of the sample. In the central part of the sample strong saturation gradients are present, while saturation plateaus are present in both the inlet end and the outlet end.

The maps indicate that a barrier to oil flow is present in the central part of the sample. The barrier is parallel to sample lamination, and is proposed because of a steep saturation gradient. Flow across the barrier seems to have occurred mainly at discrete locations along the barrier, where streaks of high $S_o$ extend into areas of low $S_o$. The streaks are mainly oriented at right angles to the barrier, i.e. at angles around 40° to the cylinder axis of the sample. In the inlet end of the sample $S_o$ is distinctly higher in the right part of the sample than in the left, indicating that oil flow occurred preferentially in this part of the sample during the oil injection step of the sample preparation.

Along most of the sample perimeter the outermost fraction of a millimetre of the sample has higher $S_o$ than sample material further inside. This in undoubtedly due to a slight evaporation of water from the sample during the physical methods comparison session described in Chapter VI. Between measurements the sample was stored in n-decane, and small amounts of evaporated water were then replaced by oil resulting in elevated $S_o$ at the margins of the sample.

The 8 mm of the sample closest to the outlet presents a uniform high $S_w$ of 92 %, with a standard deviation (SD) of 2 %. From the preparation procedure this part of the sample is known to have an $S_w$ of 100 %. The discrepancy is caused by a signal interference phenomenon similar to the one discussed under the description of the 1D saturation profile method (Chapter VI). The data shows that even though the absolute accuracy of the method is only 8 %-points for samples with water saturations close to 0 or 100 %, the relative accuracy of pixels with similar saturations is as good as 2 %-points. The mean $S_w$ in Fig.14 is 69.8 %, which should be compared with the bulk NMR determination of 76.5 % on the same day (Table II). Procedures for reducing the signal interference are currently under consideration.

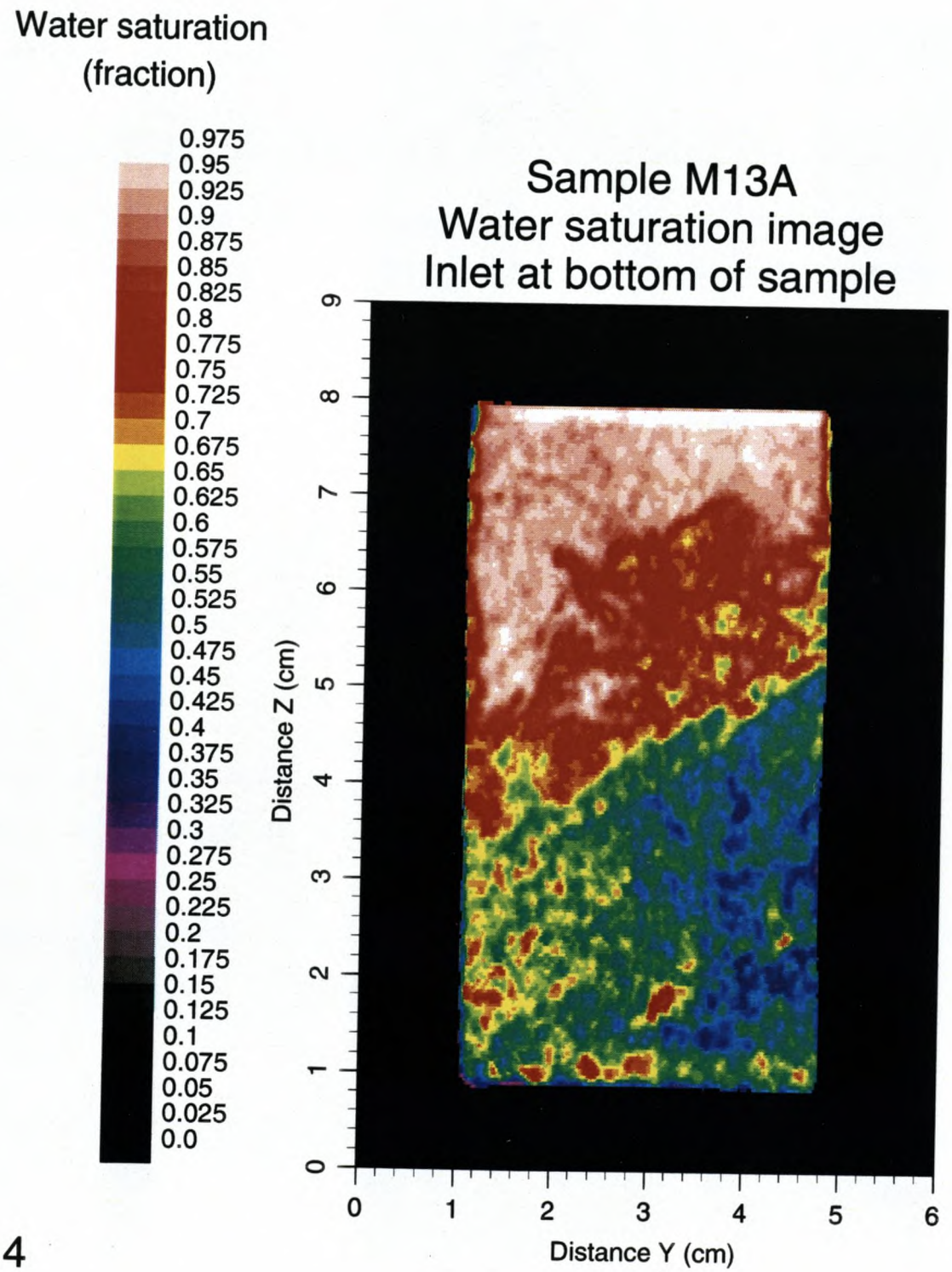


Fig. 14

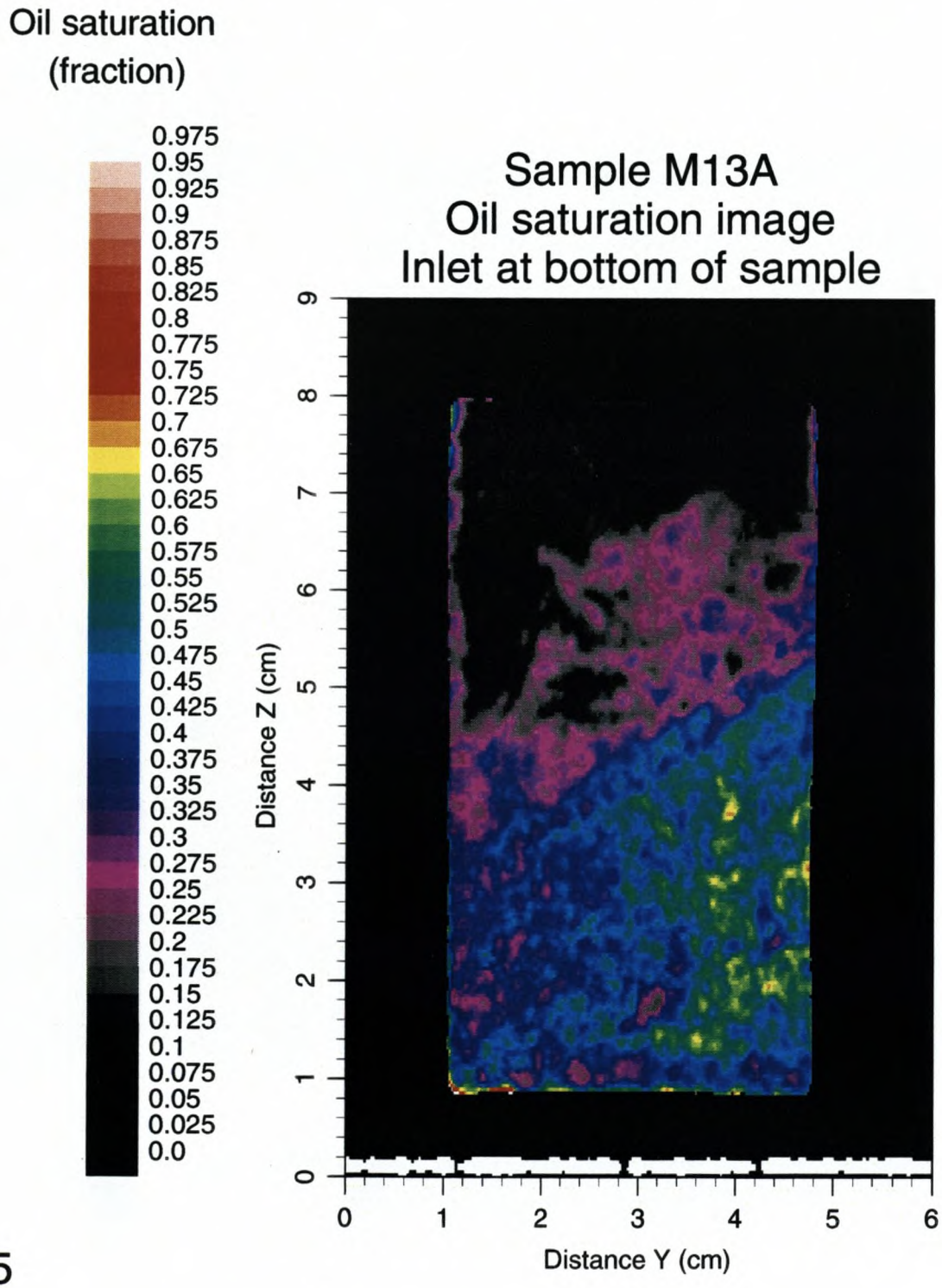


Fig. 15

Fil efgcso, 15-Apr-97, kl. 10:02:57

# VIII. Conclusions

A method for quantitative 2D mapping of porosity has been developed. The method depends on the mean porosity of the selected slice being equal to the mean porosity of the sample. Reproducibility of pixel porosities is better than 2 %-points. Spatial resolution is better than 0.8 mm. The method is demonstrated for samples with T2 constants above 8 ms, and is inferred to work for samples with T2 constants down to 5 ms.

A method for quantitative 1D saturation profile determination has been significantly improved. The method yields pixel saturations with an accuracy better than 5 %-points and a reproducibility better than 2 %-points, with a spatial resolution better than 0.8 mm. The method is demonstrated for samples with T2 constants above 8 ms, and is inferred to work for samples with T2 constants down to 3 ms.

A method for quantitative 2D mapping of saturation has been developed. Accuracy of pixel saturations is better than 8 %-points, with a reproducibility of 2 %-points. Spatial resolution is better than 2 mm. The method is demonstrated for samples with T2 constants above 10 ms, and is inferred to work for samples with T2 constants down to 8 ms.

The three methods are inferred to be applicable to most chalk samples from the Danish North Sea of Maastrichtian age. The 1D saturation profiling method has been used with success on samples of Danian and pre-Maastrichtian age.

An unsolved problem for the porosity determination method is RF coil inhomogeneity. An unsolved problem for the two saturation determination methods is interference between the water and oil signals.

# IX. References

Edelstein, W.A., Hutchison, J.M.S., Johnson, G. & Redpath, T. (1980): Spin warp NMR imaging and applications to human whole-body imaging. *Physics in Medicine and Biology, **25,4**, p.751-756, 1980.*

Edelstein, W.A., Vinegar, H.J., Tutunjian, P.N., Roemer, P.B. & Mueller, O.M.: NMR Imaging for Core Analysis. *SPE paper 18272, p.101-112, 1988.*

Halperin, W.P., D'Orazio, F., Bhattacharja, S. & Tarczon, J.C.: Magnetic resonance Relaxation Analysis of Porous Media. *In: Klafter, J. & Drake, J.M.: Molecular Dynamics in Restricted Geometries, p 311-350. John Wiley & Sons, 1989.*

Kenyon, W.E., Day, P.I., Straley, C. & Willemsen, J.F.: A Three-Part Study of NMR Longitudinal Relaxation Properties of Water-Saturated Sandstones. *SPE Formation Evaluation, **September 1988**, p.622-636, 1988.*

Kim, K-H., Chen, S., Qin, F. & Watson, A.T.: Use of NMR Imaging For Determining Fluid Saturation Distributions During Multiphase Displacements in Porous Media. *SCA Paper 9219, pp. 18, 1992.*

Nørgaard, J.V., Olsen, D., Springer, N. & Reffstrup, J. (1995): Capillary pressure curves for low permeability chalk obtained by NMR imaging of core saturation profiles. *SPE paper 30605, 1995.*

Olsen, D., Topp, S., Stensgaard, A., Nørgaard, J.V. & Reffstrup, J. (1996): Quantitative 1D saturation profiles on chalk by NMR. *Magnetic Resonance Imaging, vol.**14**, no.7, 1996.*